Non-peer reviewed preprint submitted to EarthArXiv

Title	SCI-OBS: Detection and Classification of People on the Beach and in the Surf Zone
Authors	Michael Reinwald[1], Ketron Mitchell-Wynne[1], Zane D'Amico[1], Mercedes Stringer[1], Benjamin Freeston[1]
Affiliation	[1]Surfline/Wavetrak, Inc., Huntington Beach, CA, USA
Corresponding author	Michael Reinwald <mreinwald@surfline.com>
ORCID	`https://orcid.org/0000-0001-8481-8392`
License	Creative Commons Attribution–NonCommercial 4.0 International (CC BY-NC 4.0)
Keywords	people detection; person detection; fine-grained classification; multi-class detection; beach monitoring; surfer counting; coastal video; small-object detection; YOLO; transfer learning; PTZ camera

A condensed 2-page extended abstract covering an earlier stage of this work was accepted at the 39th International Conference on Coastal Engineering (ICCE 2026), Galveston, TX, 17–22 May 2026, and is forthcoming in the conference proceedings (DOI not yet assigned). The present manuscript is substantially expanded and supersedes it as the complete account of the work.

SCI-OBS: Detection and Classification of People on the Beach and in the Surf Zone

Michael Reinwald*[1], Ketron Mitchell-Wynne[1], Zane D'Amico[1], Mercedes Stringer[1], and Benjamin Freeston[1]

[1]Surfline/Wavetrak, Inc., Huntington Beach, CA, USA

Abstract

Understanding how many people use beaches and surf zones is vital for safety, tourism, and coastal management. Traditional manual headcounts are time-consuming and inconsistent, while existing automated systems often fail in complex conditions due to glare, waves obstructing the view, and the small apparent size of distant subjects. We present SCI-OBS, an automated multi-class detector deployed on the Surfline Coastal Intelligence (SCI) pipeline's 233-camera real-time GPU inference fleet (part of a broader ∼1,200-camera archival network); this paper validates its performance on the people-detection task — detecting and counting people both on the beach and in the water — with the non-person classes (boats, jetskis, and lifeguard flags) deferred to later work. SCI-OBS is the Ultralytics YOLO26-L end-to-end detector [Ultralytics, 2025] fine-tuned on Surfline's proprietary coastal-camera dataset: tens of thousands of manually-labelled frames containing several hundred thousand labels drawn from the full diversity of Surfline's globally-distributed camera network. No coastal-specific architectural modifications were made. We validate the system on 1,400 frames from 14 representative camera sites across Australia, the United Kingdom, and the United States (64,130 ground-truth labels), benchmarking against six out-of-the-box baselines: YOLO26-L and RT-DETR-L [Zhao et al., 2024] from COCO-pretrained weights, each evaluated with and without Slicing Aided Hyper Inference (SAHI) [Akyon et al., 2022], plus MMDetection with SAHI and AWS Rekognition. SCI-OBS achieves the highest F1-score (84.0%) and recall (75.6%) of all evaluated systems while holding precision at 94.6%, and recovers on average 79.9% of the ground-truth count (mean absolute error of 9.57 individuals per frame). With each baseline evaluated at its best available operating point, none matches this precision–recall balance: the high-precision baselines reach their precision only by missing far more subjects (recovering as little as 12%), and the same architecture without coastal training reaches only 55.1% F1 (79.5% with slicing-aided inference). The gap is therefore one of training data, not architecture — closing it would require a comparable coastal-labelled corpus — and, decisively, even a detector that closed it would still emit only an undifferentiated "person" box. SCI-OBS instead resolves each detected person into a fine-grained recreation type — surfers by state, beachgoers by posture, stand-up paddleboarders — that general-purpose detectors structurally cannot produce, classifying on-sand versus in-water use with 94.4% accuracy on the same benchmark and the dominant recreation types reliably. This is what turns an undifferentiated headcount into the typed, on-sand-versus-in-water usage data that coastal-safety and management applications require.

Keywords: people detection; person detection; fine-grained classification; multi-class detection; beach monitoring; surfer counting; coastal video; small-object detection; YOLO; transfer learning; PTZ camera

1 Introduction

Understanding how people use beaches is essential for a range of coastal stakeholders — from surf businesses and tourism operators to lifeguards and local governments. Accurate usage data helps optimise staffing and safety operations, informs infrastructure planning, and unlocks insights into beachgoer and surfer behaviour. The economic stakes are real as well: recreational surfing has been shown to generate substantial annual value for the communities around individual surf breaks [Lazarow, 2007], underscoring the importance of understanding how coastal spaces are used.

Historically, beach-user data was collected through manual headcounts [Williams and Lemckert, 2007, King and McGregor, 2012, Dwight et al., 2007], which are often inaccurate, limited in coverage, and lack repeatability [Koon et al., 2021, Deacon and Kolstad, 2000, Herrera et al., 2024]. Automated video-based systems have since emerged as a promising solution, enabling continuous and high-frequency monitoring [Guillén et al., 2008, Lee et al., 2019]. Guillén et al. [2008] used Argus systems for hourly counts over four years, revealing daily, seasonal, and inter-annual usage patterns. More recently, Murray et al. [2023] used Surfline's commercial camera network and an earlier-generation version of SCI-OBS to estimate in-water surfer counts and ride durations over 2,500 hours of footage at a high-use Australian surf break.

While these studies demonstrate progress, most systems still face key challenges: limited coverage and difficulty detecting in-water users (especially surfers) due to occlusion, glare, wave interference, and the small apparent size of subjects. Aerial surveys using drone [Herrera et al., 2024] or aircraft [Provost et al., 2021] platforms can offer high-resolution snapshots over large areas but are typically conducted on a monthly or seasonal basis, limiting their applicability for continuous monitoring. In contrast, fixed coastal cameras provide a stable, long-term monitoring solution.

This paper presents SCI-OBS, the multi-class object detector of the Surfline Coastal Intelligence (SCI) pipeline, trained on a large commercial network of fixed coastal cameras and designed to operate reliably across both beaches and surf zones under varying environmental conditions. SCI-OBS produces both person classes (beachgoers, surfers, and stand-up paddleboarders) and non-person classes (boats, jetskis, and lifeguard flags). *This paper validates the person-class tasks — detection and recreation-type classification* — supporting accurate, high-frequency quantification of beach visitors, captured as typed counts on sand and in water across geographically diverse sites; the non-person class evaluation is deferred to later work. Crucially, SCI-OBS does not merely count people: it resolves them into recreation types — a surfer riding a wave versus one paddling out, a wading beachgoer versus one seated on the sand — a capability no general-purpose "person" detector provides, and the one that turns a raw headcount into the typed, on-sand-versus-in-water usage data coastal stakeholders actually need. Two implications follow, and together they frame the choice facing any group weighing an off-the-shelf detector against SCI-OBS: matching its detection accuracy is a question of training data, not architecture — requiring a comparable coastal-labelled corpus — and even a detector that matched it would still emit only an undifferentiated headcount, without the recreation-type breakdown that is SCI-OBS's reason for being. The contribution of this paper is documentary: we describe a deployed system and characterise its single-frame people-detection performance against widely-used out-of-the-box detection baselines on a manually-labelled coastal validation set. SCI-OBS's architecture is an off-the-shelf YOLO26-L with no coastal-specific modifications; the value is in the combination of coastal-domain training data and operation as a component of a larger network-scale CV pipeline, and in making the resulting performance profile available to other groups working on coastal-camera analytics. Comparison against external census ground truth (e.g. lifeguard counts, drone surveys) is out of scope here and left to future work.

The remainder of the paper is structured as follows. Section 2 situates this work against prior efforts to quantify coastal recreation from cameras. Section 3 describes the SCI pipeline and how SCI-OBS fits within it. Section 4 details the model architecture, training data, validation dataset, and evaluation metrics. Section 5 reports people-detection performance against six out-of-the-box baselines. Section 6 discusses strengths, limitations, and operational implications. Section 7 concludes.

2 Related Work

Prior work on automated coastal-recreation monitoring spans three methodological families: manual-census and survey methods, aerial / drone imagery, and fixed-camera video analysis.

2.1 Manual and survey-based counts

The foundational literature on beach attendance has relied on manual counts conducted by lifeguards, survey teams, or infrastructure operators [Williams and Lemckert, 2007, King and McGregor, 2012, Dwight et al., 2007]. These studies established the ecological, economic, and safety value of quantifying beach usage, but also documented the practical limitations: manual methods are labour-intensive, sparse in time, inconsistent across sites, and prone to observer bias [Koon et al., 2021, Deacon and Kolstad, 2000].

2.2 Aerial and drone surveys

Drone and low-altitude aerial imagery can produce high-resolution snapshots of beach usage over large areas [Herrera et al., 2024, Provost et al., 2021]. These methods are effective for episodic campaigns but are typically constrained to monthly or seasonal sampling cadence by operational and regulatory constraints, limiting their applicability for continuous monitoring or rapid response.

2.3 Fixed coastal cameras

Fixed shore-mounted cameras enable continuous, high-frequency monitoring at a single site. Within this family, early deployments used the Argus coastal-video infrastructure [Guillén et al., 2008] to produce hourly counts over multi-year observation windows. More recent work has focused on integrating modern deep-learning detectors with existing commercial camera infrastructure. Lee et al. [2019] applied vision-based safety warning systems at Haeundae Beach, Korea. Most directly related to the present work, Murray et al. [2023] used Surfline's commercial camera network and an earlier-generation version of SCI-OBS to estimate in-water surfer counts and ride durations over 2,500 hours of footage at a high-use Australian surf break.

The limitations common to this literature are well documented: difficulty detecting small, partially-occluded, or backlit subjects; sensitivity to the specific environmental and geometric conditions of each camera; and the high cost of scaling a single-site pipeline to a globally-distributed network. SCI-OBS is designed to address the third limitation by training once against the diversity of the SCI pipeline's full archival camera network rather than tuning per-site. The first two — the small/backlit/occluded subject problem — it addresses purely through coastal-domain training data, not through any architecture-side adaptation; the methodology of Section 4 details that choice.

3 System Architecture

3.1 Camera network and study sites

Surfline operates a global network of commercial pan-tilt-zoom (PTZ) surf cameras deployed at coastal locations worldwide. The full archival network (∼1,200 cameras) supplies the real-time GPU inference fleet of the Surfline Coastal Intelligence (SCI) pipeline (233 cameras across 198 spots in 21 regions), on which SCI-OBS runs continuously. The cameras are commercial IP surveillance units from a mix of vendors (including Axis, Hanwha, Dahua, and Uniview) mounted on elevated structures, with zoom and field-of-view configurable remotely.

To evaluate SCI-OBS's detection performance under varied conditions, we selected a representative subset of 14 camera sites spanning Australia, the United Kingdom, and the United States (Table 1). The selected cameras span a range of user densities, environmental conditions, and perspectives, varying in placement, view, and lighting across the network. Figure 1 shows the geographic distribution of the full camera network and example frames from the selected sites with ground-truth bounding boxes overlaid.

Table 1: Validation camera sites used in this study.

Camera	Country
Currumbin Alley	AU
Kirra	AU
Snapper Rocks	AU
Bantham	UK
Fistral	UK
Rest Bay	UK
New Smyrna	US
Steamer Lane	US
Tourmaline	US
Lower Trestles	US
Huntington Beach	US
Huntington Beach Overview	US
Middles (Saltcreek)	US
17th Street	US

3.2 Processing pipeline

Each recorded video segment is processed through the SCI pipeline, a GPU-accelerated inference stack built on NVIDIA DeepStream [NVIDIA, 2019]. Individual video segments ("rewinds") of approximately 10 minutes' duration are processed through a modular stack of neural-network and analytical models, including semantic segmentation of ocean-scene classes, visibility assessment of atmospheric conditions, the SCI-OBS detector described here, and several post-processing modules for crowd counting, wave tracking, surfer tracking, shoreline analysis, and breaking-wave-height estimation.

SCI-OBS runs on every rewind, independently of atmospheric conditions. In production, rewinds flagged by an upstream visibility classifier as degraded (fog, rain, lens spray, strong glare) are excluded from the aggregated counts exposed to customers, so the reported aggregates are robust to conditions under which per-rewind detections would be unreliable.

This paper focuses specifically on validating the per-frame people-detection performance of SCI-OBS. Cross-frame tracking, downstream post-processing, and the non-person classes are not evaluated here.

4 Methodology

4.1 Model architecture

SCI-OBS is the Ultralytics YOLO26-L end-to-end object detector [Ultralytics, 2025], a modern one-stage detector, fine-tuned on Surfline's coastal-camera dataset. We use the architecture in its publisher-supplied reference configuration, with no coastal-specific modifications of any kind. SCI-OBS's performance on the coastal-imagery distribution is therefore attributable to its training data (Section 4.2), not to any architectural adaptation.

4.2 Training data

SCI-OBS was trained on a dataset of tens of thousands of manually-labelled frames containing several hundred thousand individual labels, sourced from diverse global locations across Surfline's camera network to ensure a representative range of environmental and visual conditions. Manual annotations were created and quality-controlled by a trained analyst using a consistent labelling protocol to ensure bounding-box and class accuracy. Initial training used the full dataset; subsequent fine-tuning was prioritised on scenes where the model underperformed, with a view to improving robustness across challenging scenarios. Standard data augmentation was applied during training, including dynamic brightness, contrast, hue, and saturation adjustments to improve invariance under variable lighting

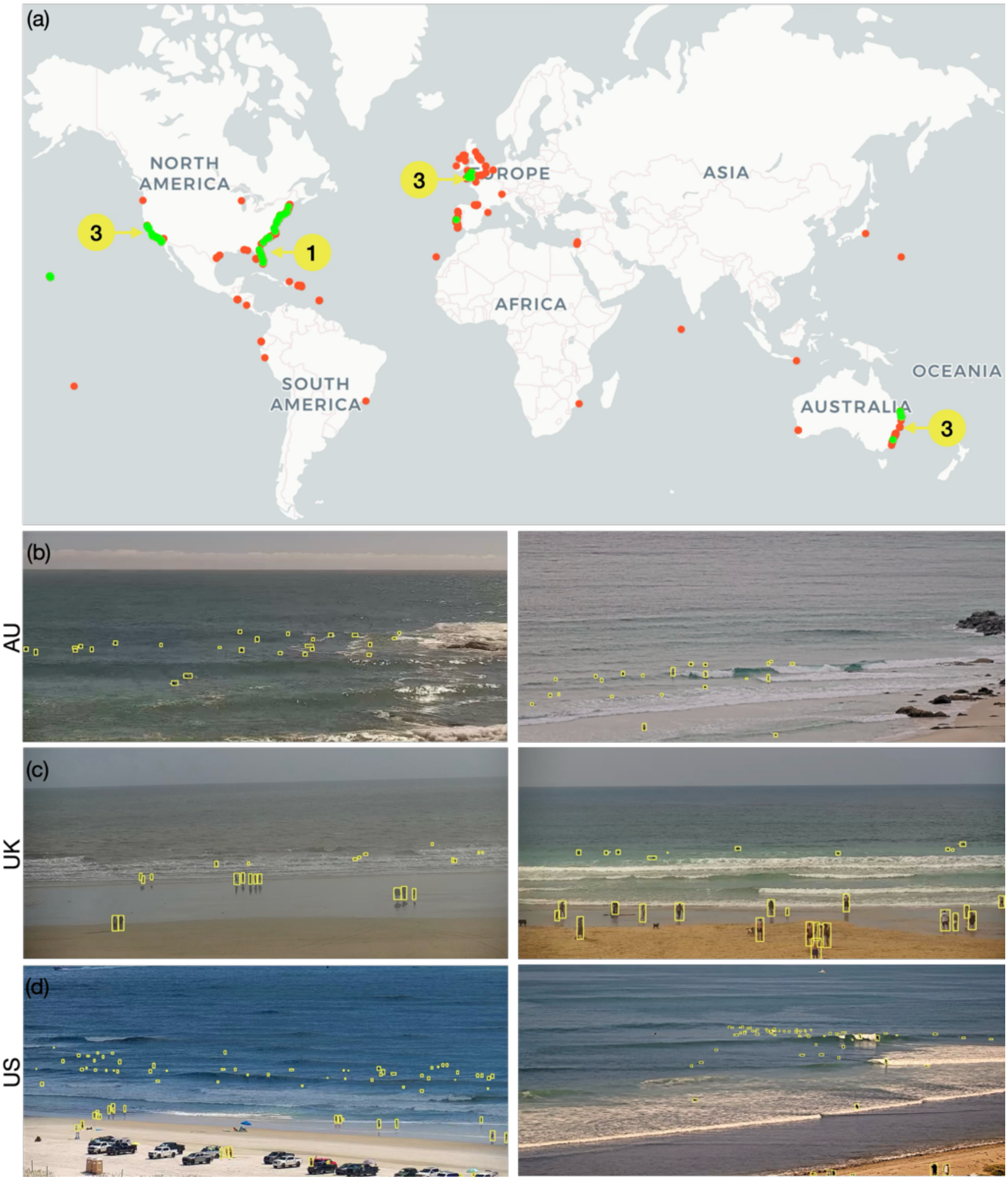

Figure 1: Overview of camera network and example detection scenes. (a) Global map showing the locations of all commercially deployed cameras (red dots) and the SCI-pipeline GPU inference fleet (green dots), with the 14 validation study sites highlighted (yellow). (b)–(d) Example frames from six representative validation sites (full list in Table 1), illustrating the variation in camera view, density, and lighting across the network: (b) AU — Snapper Rocks (left) and Kirra (right); (c) UK — Rest Bay (left) and Fistral (right); (d) US — New Smyrna (left) and Lower Trestles (right). Ground-truth person labels are shown as yellow bounding boxes.

conditions.

4.3 Class taxonomy and evaluation scope

SCI-OBS is a multi-class detector. It is trained on a set of fine-grained person classes (beachgoers in different postures — standing, sitting, lying, wading — surfers in different states — paddling, sitting, surfing — and stand-up paddleboarders) and a set of non-person classes (boats, jetskis, and lifeguard flags). *This paper validates only the person-class subset.* For the head-to-head comparison against the general-purpose baselines, all person sub-classes are collapsed into a single "People" category, making that comparison apples-to-apples (the fine-grained typing is evaluated separately in Section 5.5). The baselines structurally cannot be evaluated on the fine-grained taxonomy: their training corpora know only a single "person" class, so any apples-to-apples comparison must aggregate SCI-OBS's outputs down to that lowest common denominator. The fine-grained taxonomy is nonetheless one of SCI-OBS's operational differentiators — distinguishing wading beachgoers from sitting surfers, for example, supports downstream products that the aggregate "People" counter could not. This fine-grained typing, which the general-purpose baselines cannot produce, runs in production across the network and is evaluated quantitatively in Section 5.5; the evaluation of the non-person classes is deferred to later work. Figure 2 shows a representative SCI-OBS detection for each person class in the taxonomy.

4.4 Validation dataset

For this study, inference was applied to a controlled validation dataset consisting of 70 short video sequences: five 20-frame clips sampled at 1 Hz from each of the 14 selected camera sites described in Section 3.1. These clips were drawn from different times and scenes, yielding a total of 1,400 frames containing 64,130 ground-truth labels (an average of 45.8 people per frame). This 14-site benchmark is held out from the training pipeline: it is separate from the conventional random held-out split used for model selection during training, and the underperforming-scene prioritisation of Section 4.2 drew on training-time evaluation, not on these frames. It was curated to be representative of the network while deliberately weighting toward the dense, busy scenes that are both operationally important and the hardest case for any detector. The headline metrics are therefore measured on demanding conditions, not favourable ones.

4.5 Evaluation metrics

Three standard detection metrics assess performance: precision, recall, and F1-score. Detection outcomes are computed per frame and aggregated for overall performance. No class weighting is applied since all detections are grouped into a single "People" category. Precision (Equation 1) quantifies the proportion of true positives (TP) relative to predictions, recall (Equation 2) reflects the model's ability to recover ground-truth objects, and the F1-score (Equation 3) is the harmonic mean of precision and recall:

$$P = \frac{\mathrm{TP}}{\mathrm{TP} + \mathrm{FP}} \tag{1}$$

$$R = \frac{\mathrm{TP}}{\mathrm{TP} + \mathrm{FN}} \tag{2}$$

$$F_1 = \frac{2 \cdot P \cdot R}{P + R} \tag{3}$$

A detected bounding box is counted as a true positive when its intersection-over-union (IoU) with a ground-truth box exceeds a threshold. For the analysis below, we report metrics at an IoU threshold of 0.1. This choice is motivated by the downstream task: SCI-OBS feeds a per-frame counting and aggregation pipeline, for which a detection only needs to be uniquely associable with a ground-truth instance — localisation fidelity beyond rough overlap carries no operational benefit. Matching is performed 1:1 (each prediction can claim at most one ground-truth box, and vice versa, by greedy assignment on best IoU), so a low threshold does not enable double-counting in dense scenes.

4.6 Benchmark models

SCI-OBS was benchmarked against six out-of-the-box detectors evaluated on the same validation dataset using their publishers' reference weights with no coastal fine-tuning:

1. **YOLO26-L (COCO-only)** [Ultralytics, 2025] — the same architecture as SCI-OBS, loaded from publisher-supplied COCO-pretrained weights rather than coastally fine-tuned. Referred to as YOLO26-L (and YOLO26-L + SAHI for the SAHI-enhanced variant).

2. **RT-DETR-L (COCO-only)** [Zhao et al., 2024] — a state-of-the-art transformer-based detector from its publisher-supplied COCO-pretrained weights. Referred to as RT-DETR-L (and RT-DETR-L + SAHI).

3. **MMDetection** with SAHI [Akyon et al., 2022], referred to as MMDET-SAHI.

4. **AWS Rekognition**.

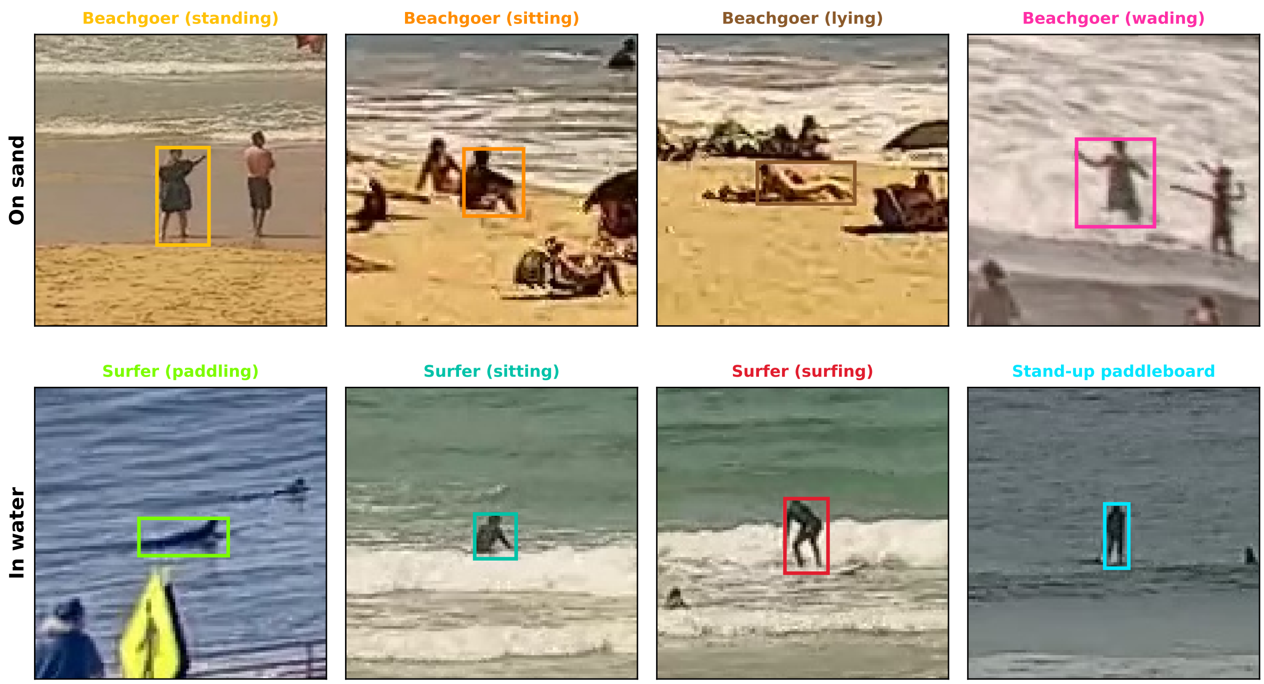

Figure 2: Representative SCI-OBS detections for the person classes in the fine-grained taxonomy, grouped into on-sand beachgoers (standing, sitting, lying, wading) and in-water users (surfers paddling, sitting, and surfing; stand-up paddleboarders). Each crop shows a single predicted detection; box colour and label give the predicted class. The general-purpose baselines emit a single undifferentiated "person" box for every one of these subjects; resolving them into recreation types is what supports on-sand-versus-in-water utilisation and mode-of-recreation breakdowns. These crops are illustrative; per-class classification accuracy is quantified in Section 5.5.

The YOLO26-L pair is the sharpest comparison: it is the same detector architecture as SCI-OBS but trained on the COCO general-purpose dataset rather than on Surfline's coastal data. Any performance gap between SCI-OBS and YOLO26-L is therefore attributable to training data alone, not to architectural differences. The RT-DETR-L pair extends the comparison to a different modern architecture family (transformer-based) to confirm that the pattern is not architecture-specific. SAHI (Slicing Aided Hyper Inference) [Akyon et al., 2022] variants apply image tiling (512×512 slices with 0.2 overlap) at inference time, which is the standard technique for improving small-object detection without re-training. MMDET-SAHI and AWS Rekognition are retained from earlier evaluations as additional points of reference: a different open-source framework and a widely-used commercial service, respectively. SCI-OBS and the YOLO26-L and RT-DETR-L baselines (with and without SAHI) were run with Ultralytics 8.4.38 and SAHI 0.11.36. Evaluation against vision–language foundation models prompted for counting (e.g. Gemini, Claude Opus) is deferred to future work.

Each detector was evaluated at its F1-optimal confidence threshold, chosen per model by sweeping the score threshold over $[0.1, 0.7]$ against the validation set at IoU 0.1 and selecting the value that maximises F1. Reporting every model at its own best operating point removes the confidence-threshold choice as a confound, so the remaining differences reflect the detectors and their training rather than an arbitrarily-set threshold. This selection is made on the validation set itself, so each baseline is shown at a best-case operating point fitted to the evaluation data; SCI-OBS is shown at the fixed production threshold configuration it runs at on the live fleet, which the same sweep confirmed coincides with its F1-optimum on this set. Every model, SCI-OBS included, is therefore compared at its test-set F1-optimal operating point. Two baselines whose stored predictions are floored above 0.1 — MMDET-SAHI (floor 0.40) and AWS Rekognition (floor 0.55) — are reported at that floor; both are recall-limited, so a higher threshold could only further reduce their already-low recall.

5 Results

5.1 Detection performance

SCI-OBS achieves the highest F1-score (84.0%) and the highest recall (75.6%) of all evaluated models at the IoU 0.1 operating point, while holding precision at 94.6% (Figure 3 and Table 2); each detector is evaluated at its own F1-optimal confidence threshold, so the comparison reflects every model at its best operating point. The SAHI-tiled baselines come closest on both axes: YOLO26-L + SAHI pairs high precision (93.2%) with lower recall (69.3%), and RT-DETR-L + SAHI balances 82.4% precision against 70.9% recall — but both trail SCI-OBS on F1 (79.5% and 76.2%). The remaining baselines sacrifice recall for precision: AWS Rekognition is highly precise (97.5%) but recovers only 12% of subjects, and the non-tiled baselines miss 53–60% of people. The single most informative comparison is between SCI-OBS and YOLO26-L — the same detector architecture, distinguished only by training data: SCI-OBS outperforms it by 28.9 F1 points, and even YOLO26-L + SAHI, which gives the out-of-the-box detector substantially more per-object pixel budget through image tiling, still trails by 4.5 points. The RT-DETR-L pair confirms the pattern holds across architecture families: tiling lifts it from 52.1 to 76.2 F1, but coastal training is what carries SCI-OBS the rest of the way to 84.0. SCI-OBS's coastal-specific training data is what delivers high recall without sacrificing precision.

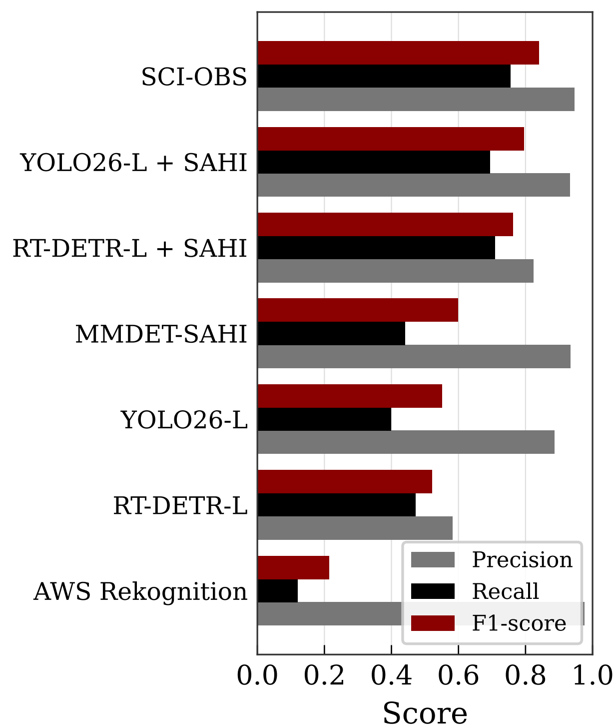

Figure 3: Detection metrics (precision, recall, and F1-score) for SCI-OBS and the six out-of-the-box benchmark models at IoU threshold 0.1, each evaluated at its F1-optimal confidence threshold. SCI-OBS has the highest recall and F1; the SAHI-tiled YOLO26-L and RT-DETR-L are the only baselines that approach it on both axes, while the non-tiled baselines and AWS Rekognition hold high precision only by missing most subjects.

Table 2: Per-frame detection metrics on the 1,400-frame validation dataset (14 sites, 64,130 ground-truth labels) at IoU threshold 0.1. Rows ordered by F1.

Model	P	R	F1
SCI-OBS	94.6	75.6	**84.0**
YOLO26-L + SAHI	93.2	69.3	79.5
RT-DETR-L + SAHI	82.4	70.9	76.2
MMDET-SAHI	93.4	44.0	59.8
YOLO26-L	88.6	39.9	55.1
RT-DETR-L	58.2	47.1	52.1
AWS Rekognition	97.5	12.0	21.3

5.2 Count recovery

To assess the models' accuracy in estimating the number of people present — the quantity of primary operational interest — predicted frame-level counts were compared with ground-truth counts (Figure 4). We report two summary statistics: mean absolute error (MAE) between predicted and actual counts, and an aggregate count-recovery rate, defined as the total number of detected individuals divided by the total number of ground-truth individuals across all frames. Neither statistic is decisive on its own: a model can post an accurate aggregate count by letting within-frame false positives cancel missed detections, so we read both alongside the miss/false-positive decomposition of Section 5.3.

SCI-OBS recovers 79.9% of the ground-truth count (MAE 9.57 individuals per frame) at a low false-positive rate (2.0 per frame — the lowest among the high-recall detectors; Section 5.3). Most out-of-the-box baselines systematically underestimate: YOLO26-L (MAE 25.39, recovery 45.0%) and MMDET-SAHI (MAE 24.24, recovery 47.1%) miss roughly half the subjects, AWS Rekognition recovers only 12.3% (MAE 40.19), and YOLO26-L + SAHI, the strongest CNN baseline, reaches recovery 74.4% (MAE 12.14) but still trails SCI-OBS. At its F1-optimal threshold, RT-DETR-L + SAHI actually attains the lowest count MAE of any model (9.18, recovery 86.0%), marginally below SCI-OBS's — but it does so while firing 6.9 false positives per frame, more than three times SCI-OBS's rate (Section 5.3). Its accurate aggregate count arises substantially from false detections offsetting missed subjects within the same frames, rather than from correct detections. SCI-OBS reaches comparable count accuracy through reliable detection — the highest F1 and recall at a low false-positive rate — which is what the downstream tracking-and-aggregation pipeline depends on, rather than through compensating errors.

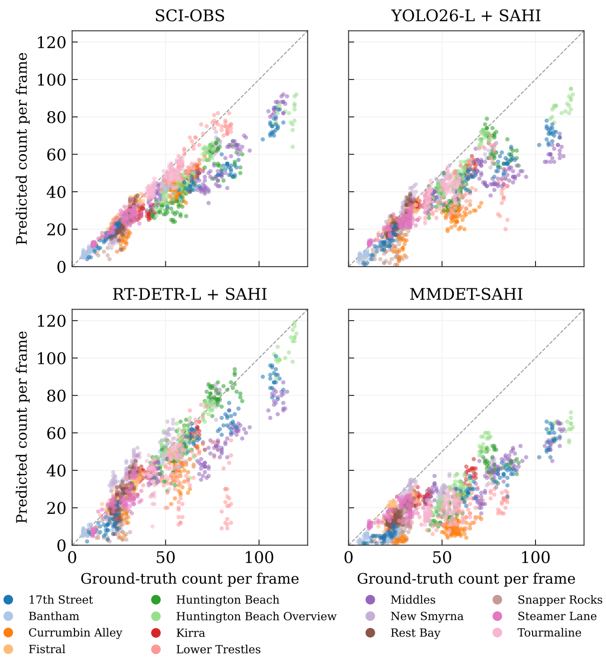

Figure 4: Per-frame predicted counts vs. ground-truth counts for SCI-OBS and the three strongest baselines (YOLO26-L + SAHI, RT-DETR-L + SAHI, MMDET-SAHI). Each point is one frame from the 1,400-frame validation set; colour encodes the camera site. SCI-OBS predictions track the identity line closely across sites and count magnitudes; the CNN-based baselines (YOLO26-L + SAHI and MMDET-SAHI) sit below the identity line, undercounting. RT-DETR-L + SAHI, at its F1-optimal threshold, also tracks the line closely on aggregate, but reaches that count balance with a markedly higher false-positive rate (Section 5.3) — false detections offsetting missed subjects rather than correct detections. The three baselines not shown here (the no-SAHI YOLO26-L and RT-DETR-L variants and AWS Rekognition) all lie further from the identity line; see Table 2 for their numerical results.

5.3 Per-frame miss/false-positive pattern

Decomposing the errors into misses and false positives clarifies the operational profile of each model. SCI-OBS averages 11.2 missed detections and 2.0 false positives per frame (against a mean of 45.8 ground-truth people per frame) — the best of both. YOLO26-L + SAHI is the closest baseline operating point (14.1 misses, 2.3 false positives). The conservative baselines miss far more while rarely firing spuriously: MMDET-SAHI averages 25.6 misses against 1.4 false positives, YOLO26-L 27.5 against 2.3, and AWS Rekognition 40.3 against 0.1. Even at their F1-optimal thresholds the transformer baselines retain a higher false-positive rate than the CNN detectors: RT-DETR-L + SAHI averages 13.4 misses and 6.9 false positives per frame, and RT-DETR-L 24.2 misses against 15.5 false positives. SCI-OBS achieves the highest recall — the fewest misses of any model — at the lowest false-positive rate among the high-recall detectors, which is the right operating point for total-count estimation feeding a tracking-and-aggregation pipeline.

5.4 Qualitative examples

Figure 5 shows the highest-density frame at each of three representative sites (Lower Trestles, Tourmaline, Fistral) with ground-truth bounding boxes alongside three model predictions overlaid: SCI-OBS, YOLO26-L + SAHI, and RT-DETR-L + SAHI. The dense Lower Trestles frame (top row, GT $n = 85$) is the most informative comparison: SCI-OBS recovers $n = 76$ subjects, while the same architecture without coastal training, even with SAHI tiling, recovers only $n = 25$. The qualitative pattern matches the aggregate F1: the gap between SCI-OBS and YOLO26-L + SAHI is small on the easier, lower-density frames (Tourmaline and Fistral) and large on the dense surf-line frames where the bulk of the validation labels live.

5.5 Recreation-type classification

Detecting people is necessary but not sufficient: the operational value of SCI-OBS lies in resolving each detected person into a fine-grained recreation type — a capability the general-purpose baselines structurally lack, since their training corpora recognise only an undifferentiated “person.” Every ground-truth box in the validation set carries a manually-assigned recreation state (Section 4.4), so we evaluate this typing on the same 14-site benchmark. We report *classification given detection*: of the people SCI-OBS detects (matched to a ground-truth box at IoU 0.1, class-agnostically — i.e., by spatial overlap alone), how often the predicted class equals the ground-truth class. This isolates typing quality from the detection recall of Section 5.1.

The operationally decisive distinction — on-sand versus in-water use — is recovered with **94.4% accuracy**: a detected beachgoer is almost never mistaken for a water user (Figure 6). The residual cross-block confusion is not spread across the sand/water boundary but concentrates at the sitting-surfer/wading waterline interface — where upright people stand at the water’s edge — the single place the two groups are genuinely hard to separate. This is precisely the breakdown that turns a raw headcount into on-sand-versus-in-water utilisation data, and no general-purpose “person” detector can produce it at all.

At the finer eight-class level, overall accuracy is 75.8%, concentrated in the dominant types: standing beachgoers (96%), sitting surfers (86%), and sitting beachgoers (85%) are typed reliably. The residual confusions fall almost entirely between visually similar poses *within* the same on-sand or in-water group: lying beachgoers are often read as sitting, wading beachgoers — standing in shallow water — as standing (67%), and paddling surfers and stand-up paddleboarders as sitting surfers (36% and 55%). These reflect genuine pose ambiguity at coastal-camera range rather than confusion across the sand/water boundary. Ongoing work targets these in-block confusions: the most direct lever is fusing SCI-OBS’s detections with the SCI pipeline’s semantic-segmentation outputs, which make the water/sand boundary explicit at the pixel level — exactly the signal needed to separate wading beachgoers from those standing on dry sand — and analogous strategies are in development for the other weak classes. A fully supervised per-class study, including SCI-OBS’s non-person classes, is left to later work.

6 Discussion

6.1 Why domain-specific training wins here

The performance gap between SCI-OBS and the general-purpose benchmarks is larger than is typically seen when comparing detection architectures on natural-image benchmarks such as COCO. Because each model is evaluated at its own F1-optimal confidence threshold, the gap is not an artefact of operating-point choice; we attribute it to the training distribution:

- **Same architecture, with vs. without coastal training.** The cleanest evidence is the YOLO26-L comparison. SCI-OBS and YOLO26-L are the same detector architecture; the only difference between them is the training data SCI-OBS was fine-tuned on. The F1 gap is 28.9 points (84.0 vs. 55.1). Tiling — the standard inference-time technique to give detectors more per-object pixel budget — helps YOLO26-L + SAHI substantially (55.1 → 79.5 F1) but still leaves a 4.5-point

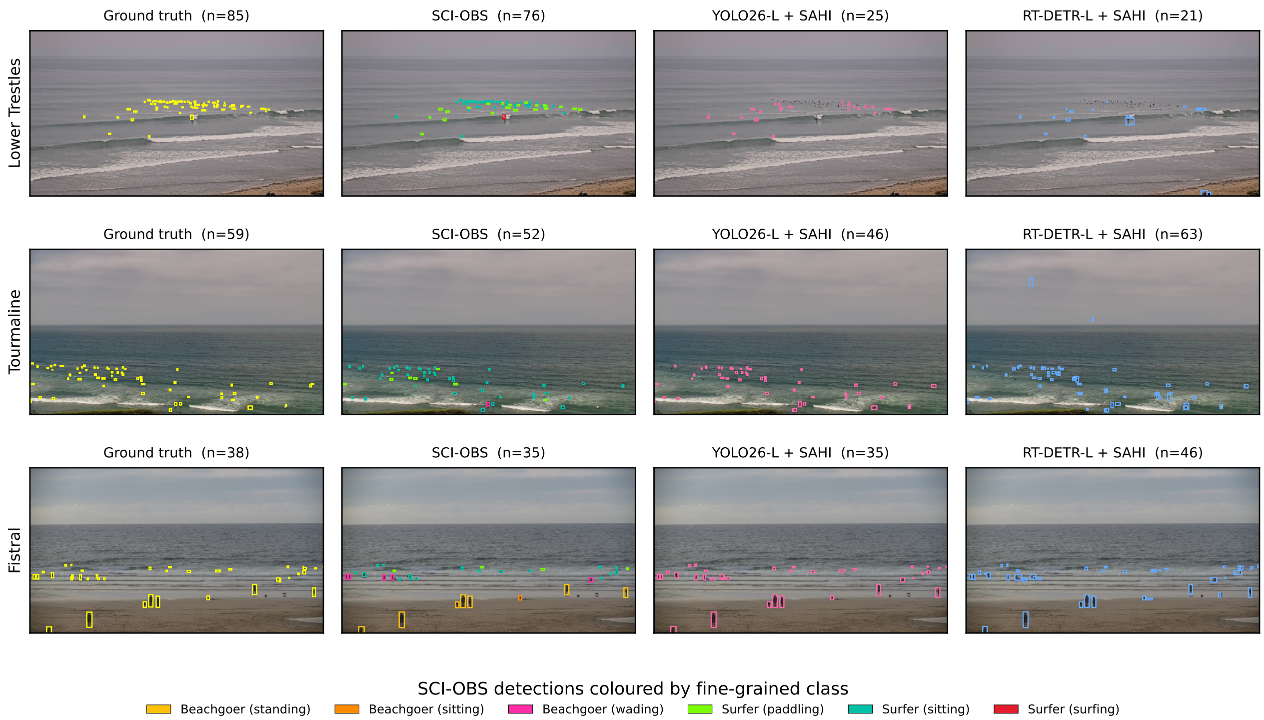

Figure 5: Bounding-box overlays on the highest-GT-density frame at each of three representative sites — (top) Lower Trestles, (middle) Tourmaline, (bottom) Fistral. Columns: ground truth (yellow), SCI-OBS (coloured by fine-grained class, legend below), YOLO26-L + SAHI (pink), RT-DETR-L + SAHI (blue). Per-panel counts (n) match the underlying validator data used elsewhere in this paper. SCI-OBS tracks the ground truth closely while the out-of-the-box detectors fall progressively further behind as scene density increases; the SCI-OBS box colours additionally show that it types each recovered subject by recreation class, which the baselines — emitting only undifferentiated boxes — structurally cannot.

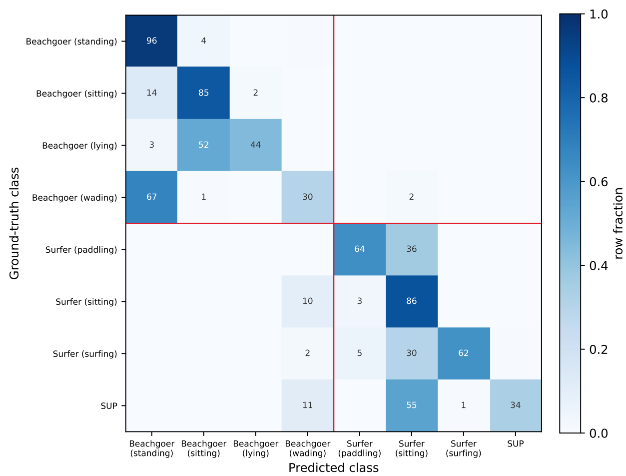

Figure 6: Recreation-type classification of SCI-OBS over the people it detects, as a row-normalised confusion matrix (percentage of each ground-truth class; rows sum to 100). Red lines separate the on-sand classes (top-left block) from the in-water classes (bottom-right block): cross-block confusion is rare (94.4% on-sand/in-water accuracy), concentrated at the sitting-surfer/wading waterline interface, while the larger per-class confusions lie between visually similar poses within a block. General-purpose detectors emit only an undifferentiated "person" and cannot populate this matrix.

gap that only fine-tuning closes. The RT-DETR-L pair shows the same pattern holds across architecture families: the transformer detector is unaffected by the architectural choice but bound by the training distribution.

- **Coastal-domain training data.** SCI-OBS is trained on tens of thousands of manually-labelled frames and several hundred thousand labels sampled from the full diversity of Surfline's camera network — spanning viewing geometries, lighting conditions, water states, and densities that do not appear at useful frequency in any general-purpose training corpus. The benchmark systems' failure mode is not a weakness of the underlying detector architectures but of their training distributions: out-of-the-box detectors trained predominantly on COCO-scale subjects in road and indoor scenes have not seen enough small, water-occluded, backlit human subjects to learn to detect them, regardless of how the inference is configured. We expect any reasonably modern detector retrained on SCI-OBS's data to substantially close the gap; conversely, no out-of-the-box detector will close it without retraining. The validation set is, by design, in-domain for SCI-OBS— drawn from the same camera network, viewing geometries, and conditions it was trained to operate on. This is not a confound to discount but the central finding: the performance bar reported here is reachable only by a detector trained on comparable coastal data, so acquiring that data — not selecting a better architecture — is the binding constraint for anyone seeking to match it.

- **Operating-point choice.** Reporting metrics at IoU 0.1 reflects the downstream consumer of SCI-OBS's outputs — a per-frame counting and aggregation pipeline that requires a detection to be uniquely associable with a subject but does not benefit from sub-pixel localisation. Strict-IoU evaluation (IoU $\geq$ 0.7) would penalise all evaluated models on the small, partially-occluded coastal subjects, but that strictness has no operational relevance to the counting task.

6.2 Operational advantages

Beyond the aggregate detection metrics reported above, SCI-OBS offers operational advantages that translate to practical value for coastal stakeholders. The system operates across many brands of commercial PTZ CCTV cameras with minimal manual intervention, which is what makes network-scale deployment tractable. Unlike drone-based surveys that provide episodic snapshots, or manual counting methods that are labour-intensive and error-prone, SCI-OBS enables continuous, high-frequency monitoring that captures the dynamic nature of beach-usage patterns over days, weeks, and seasons. Most importantly, an accurate headcount is necessary but not sufficient for most coastal-management and safety applications: how many people are present matters less than what they are doing and where. SCI-OBS classifies each detected person by recreation type — separating on-sand from in-water use with 94.4% accuracy, and typing the dominant beachgoer and surfer states reliably (Section 5.5) — which the general-purpose baselines structurally cannot, regardless of how much inference compute they are given. This is the decisive practical difference for a practitioner weighing an off-the-shelf detector against SCI-OBS, and the gap is three-fold. Matching SCI-OBS's detection accuracy would itself require fine-tuning on a large coastal-labelled corpus (here, several hundred thousand labels); the strongest baselines only approach it after per-dataset confidence-threshold tuning and slicing-aided inference at several times the compute cost; and even then the output is an undifferentiated "person" count, with none of the on-sand-versus-in-water or mode-of-recreation breakdowns the downstream products require. Figure 7 shows this typing running across representative sites and conditions.

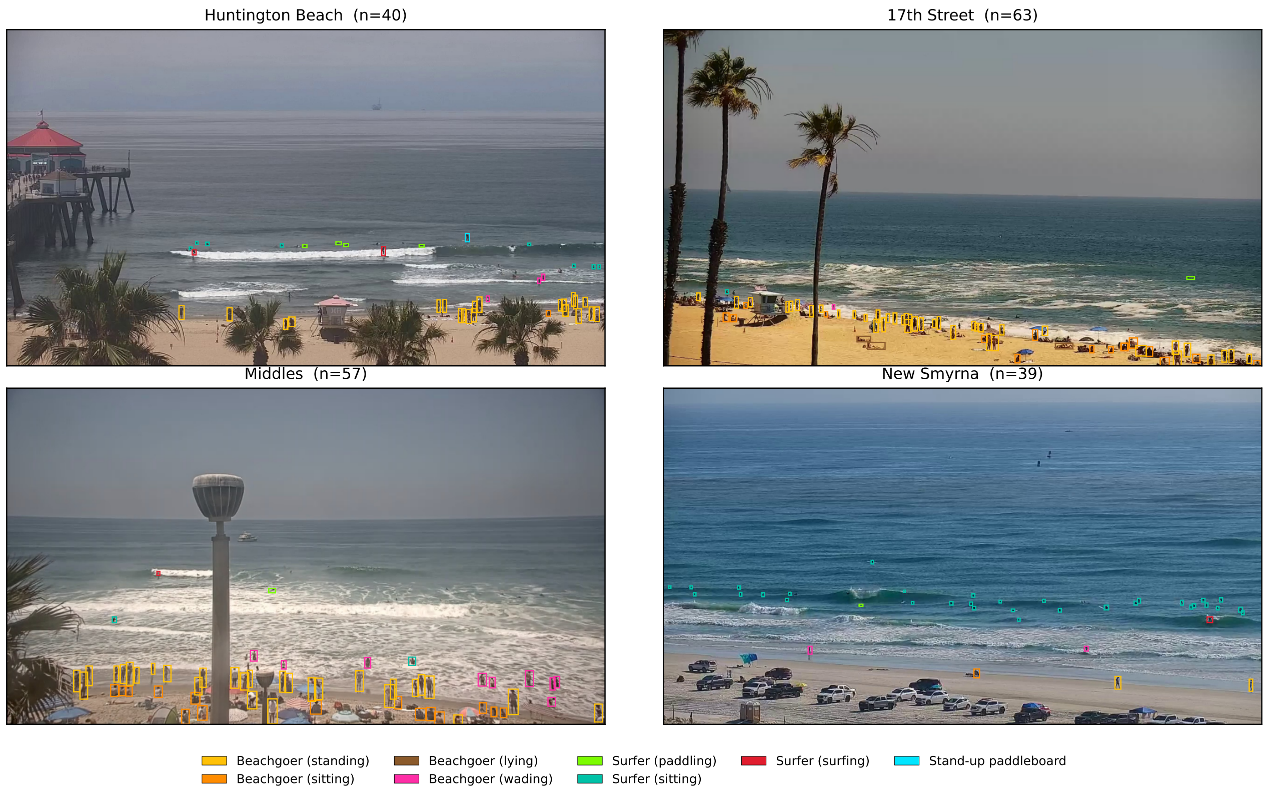

Figure 7: SCI-OBS fine-grained class predictions across four representative sites and conditions (Huntington Beach, 17th Street, Middles, New Smyrna). Every SCI-OBS person detection is drawn and coloured by its predicted class (legend); the on-sand beachgoer classes (warm tones) and in-water surfer/SUP classes (cool tones) separate cleanly by colour, illustrating that the taxonomy holds across views, lighting, and densities. Per-panel n is the SCI-OBS person count. Examples are illustrative; per-class classification accuracy is quantified in Section 5.5.

6.3 Limitations

Single-frame evaluation. This study focuses on single-frame detection performance. Cross-frame temporal consistency, tracking, and count-deduplication behaviour are not evaluated here; both are handled by downstream post-processing modules of the SCI pipeline and are outside the scope of this paper.

Clear-visibility evaluation only. The validation frames were drawn from sessions under clear visibility conditions. Per-rewind detection performance under extreme weather — heavy fog, rain, lens spray, strong glare — is not characterised in this study. In production deployment, SCI-OBS still runs on those rewinds; downstream aggregation excludes rewinds flagged as degraded from reported counts, so the aggregate counts exposed to customers are robust to those conditions even though per-rewind performance in them is not measured here. A visibility-stratified evaluation of per-rewind detection performance is a natural extension.

Detection scope versus classification. The headline *detection* metrics (Section 5.1) collapse the fine-grained person classes to a single "People" class, to enable a like-for-like comparison with general-purpose detectors that do not share the taxonomy; the fine-grained *typing* is evaluated separately in Section 5.5, as classification accuracy given detection over the well-populated person classes. A fuller treatment — full per-class precision and recall, and evaluation of SCI-OBS's non-person classes (boats, jetskis, and lifeguard flags) — is deferred to later work.

No per-site disaggregation. Aggregate metrics across 14 sites hide per-site variation. A few sites (Tourmaline, Lower Trestles, the Huntington Beach overview) have consistently high subject counts and dense scenes that drive most of the aggregate error budget; performance on lower-density sites is higher than the aggregate numbers suggest.

7 Conclusion

We have characterised the people-detection and recreation-type classification performance of SCI-OBS, the multi-class object detector of the Surfline Coastal Intelligence (SCI) pipeline, against six out-of-the-box benchmark detectors on a 1,400-frame, 14-site validation dataset. SCI-OBS achieves the highest F1-score (84.0%) and recall (75.6%) and recovers 79.9% of the ground-truth count (mean absolute error 9.57 individuals per frame). The strongest baseline — the same CNN architecture with SAHI but trained on COCO rather than Surfline's coastal data — reaches F1 79.5%, 4.5 points below SCI-OBS; without SAHI the same architecture drops to 55.1%, a 28.9-point gap closed entirely by coastal-domain fine-tuning. Beyond detection, SCI-OBS types the people it detects — separating on-sand from in-water use with 94.4% accuracy — which no general-purpose "person" detector can do.

The contribution of this paper is documentary: SCI-OBS is a modern off-the-shelf detector used in its reference configuration, with no coastal-specific architectural modifications. The same-architecture comparison — coastal fine-tuning against COCO-only weights — isolates the cause of SCI-OBS's performance advantage to its training data; tiling-based inference techniques narrow but do not close the gap. The practical corollary is that no out-of-the-box detector is likely to match SCI-OBS without retraining on a comparable dataset. SCI-OBS is already in production, feeding the recreational-user counts exposed through SCI's B2B platform.

Future work falls in two categories:

- **Validation extensions**: cross-frame temporal consistency evaluation; visibility-stratified performance characterisation; full per-class precision/recall and the non-person classes, beyond the aggregate classification reported in Section 5.5.

- **Comparisons and dataset growth**: comparison against general-purpose vision–language foundation models (e.g. Gemini, Claude Opus) prompted for coastal-scene counting, to test whether the scale of pretraining offsets the domain-specific training advantage demonstrated here; active-learning loops that prioritise annotation effort toward systematically-missed scenes; and domain adaptation as new camera sites are added to the network.

Together, these results indicate that domain-specific training data, more than architecture novelty, is the principal lever for high-recall people detection on operational coastal-camera networks — and that the resulting model pairs the best-balanced detection among the systems evaluated (the highest recall and F1 at a low false-positive rate) with a capability no out-of-the-box detector offers: a breakdown into the recreation types that turn a count into actionable coastal-usage data. Performance on SCI-OBS's non-person classes (boats, jetskis, and lifeguard flags) is left to later work.

Author disclosure

B. Freeston, a co-author of this paper, is the named inventor on US Patent 10,891,481 B2 (Freeston [2021]), assigned to Surfline/Wavetrak, Inc., which discloses the broader automated ocean-sensing framework within which SCI-OBS was developed.

Competing interests

All authors are employees of Surfline/Wavetrak, Inc., which develops and commercially operates the SCI pipeline and the SCI-OBS detector evaluated in this paper.

Data and code availability

The training dataset and the fine-tuned model weights are proprietary and are not released. The base architecture (Ultralytics YOLO26-L, used in its reference configuration with no modifications), the validation-dataset composition (14 camera sites, 1,400 frames, 64,130 labels), and the evaluation protocol described in this paper are sufficient for independent re-implementation against a comparable dataset.

References

Fatih Cagatay Akyon, Sinan Onur Altinuc, and Alptekin Temizel. Slicing aided hyper inference and fine-tuning for small object detection. *2022 IEEE International Conference on Image Processing (ICIP)*, pages 966–970, 2022. doi: 10.1109/ICIP46576.2022.9897990.

Robert T. Deacon and Charles D. Kolstad. Valuing beach recreation lost in environmental accidents. *Journal of Water Resources Planning and Management*, 126(6):374–381, 2000. doi: 10.1061/(ASCE)0733-9496(2000)126:6(374).

Ryan H. Dwight, Mitchell V. Brinks, G. SharavanaKumar, and Jan C. Semenza. Beach attendance and bathing rates for Southern California beaches. *Ocean & Coastal Management*, 50(10):847–858, 2007. doi: 10.1016/j.ocecoaman.2007.04.002.

Benjamin Freeston. Automated detection of features and/or parameters within an ocean environment using image data. United States Patent and Trademark Office, 2021. US Patent 10,891,481 B2, assigned to Surfline/Wavetrak, Inc.

Jorge Guillén, Antonio García-Olivares, Elena Ojeda, Andres Osorio, Óscar Chic, and Raul González. Long-term quantification of beach users using video monitoring. *Journal of Coastal Research*, 24(6):1612–1619, 2008. doi: 10.2112/07-0886.1.

César Herrera, Rod M. Connolly, Jasmine A. Rasmussen, Gerrard McNamara, Thomas P. Murray, Sebastian Lopez-Marcano, Matthew Moore, Max D. Campbell, and Fernando Alvarez. Drone insights: unveiling beach usage through AI-powered people counting. *Drones*, 8(10), 2024. doi: 10.3390/drones8100579.

Philip King and Andrew McGregor. Who's counting: an analysis of beach attendance estimates and methodologies in southern California. *Ocean & Coastal Management*, 58:17–25, 2012. doi: 10.1016/j.ocecoaman.2011.12.005.

William Koon, Andrew Schmidt, Ana Catarina Queiroga, Justin Sempsrott, David Szpilman, Jonathon Webber, and Robert Brander. Need for consistent beach lifeguard data collection: results from an international survey. *Injury Prevention*, 27(4):308–315, 2021. doi: 10.1136/injuryprev-2020-043793.

Neil Lazarow. The value of coastal recreational resources: a case study approach to examine the value of recreational surfing to specific locales. *Journal of Coastal Research*, 50(sp1):12–20, 2007. doi: 10.2112/JCR-SI50-003.1.

Jooyong Lee, Jisoo Park, Inchul Kim, and Dae Young Kang. Application of vision-based safety warning system to Haeundae beach, Korea. *Journal of Coastal Research*, 91(SI):216–220, 2019. doi: 10.2112/SI91-044.1.

Tom Murray, Megan Greaves, Guilherme Da Silva, Oliver Boyle, Ketron Wynne, Ben Freeston, Luke Ditria, Paul Jardine, Ellen Ditria, Darrell Strauss, Rodger Tomlinson, and Paul Burton. Utilising object detection from coastal surf cameras to assess surfer usage. In *Australasian Coasts & Ports Conference 2023*, Sunshine Coast, QLD, Australia, 2023. doi: 10.3316/informit.472912089750558.

NVIDIA. DeepStream SDK: Accelerating real-time ai-based video and image analytics. NVIDIA Developer Technical Documentation, `https://developer.nvidia.com/deepstream-sdk`, 2019.

Euan J. Provost, Melinda A. Coleman, Paul A. Butcher, Andrew Colefax, Thomas A. Schlacher, Melanie J. Bishop, Rod M. Connolly, Ben L. Gilby, Christopher J. Henderson, Alan Jones, Mariano Lastra, Brooke Maslo, Andrew D. Olds, and Brendan P. Kelaher. Quantifying human use of sandy shores with aerial remote sensing technology: the sky is not the limit. *Ocean & Coastal Management*, 211:105750, 2021. doi: 10.1016/j.ocecoaman.2021.105750.

Ultralytics. Ultralytics yolo. Open-source software, `https://github.com/ultralytics/ultralytics`, 2025. YOLO26 model family.

Paul Williams and Charles Lemckert. Beach carrying capacity: has it been exceeded on the Gold Coast? *Journal of Coastal Research*, 50(sp1):21–24, 2007. doi: 10.2112/JCR-SI50-004.1.

Yian Zhao, Wenyu Lv, Shangliang Xu, Jinman Wei, Guanzhong Wang, Qingqing Dang, Yi Liu, and Jie Chen. DETRs beat YOLOs on real-time object detection. In *IEEE/CVF Conference on Computer Vision and Pattern Recognition (CVPR)*, 2024.